View metadata, citation and similar papers at core.ac.uk
brought to you by CORE
provided by CiteSeerX

Proceedings of IMECE2006
2006 ASME International Mechanical Engineering Congress and Exposition
November 5-10, 2006, Chicago, Illinois, USA

IMECE2006-15042

A MEMS-BASED MICRO HEAT ENGINE WITH INTEGRATED THERMAL SWITCH

L.W. Weiss, J.H.Cho, D.J. Morris, D.F. Bahr, C.D. Richards, and R.F. Richards
School of Mechanical and Materials Engineering
Washington State University, Pullman, WA, USA

ABSTRACT

This work details the effect of top membrane compliance on the performance of a MEMS based micro-heat engine and integrated thermal switch at operating speeds of 20, 40, and 100Hz and heat inputs of up to 60mJ per cycle. The engine consists of two flexible membranes encapsulating a volume of saturated working fluid. A thermal switch is used to intermittently reject heat from the engine to a constant temperature cooling sink. Mechanical work output is measured based on the engine's top membrane deflection and internal operating pressure. Three top membranes are considered; a 2micron thick silicon membrane, a 300nm thick silicon-nitride membrane, and a 3micron thick corrugated silicon membrane. The engine is shown to produce 1.0mW of mechanical power when operated at 100Hz.

INTRODUCTION

The success of MEMS based sensors and actuators have generated a need for small, energy dense power generation systems to power them. This need has driven the development of a wide array of micro-power approaches and associated power generation devices. These have included a gas turbine (Brayton cycle) engine [1], a Homogeneous Charge Compression Ignition Free Piston (Otto cycle) Engine [2], and a micro rotary internal combustion (Otto cycle) engine [3]. All three of these devices are internal combustion engines. Work at our lab has focused on an external combustion system that is capable of converting low-grade heat energy to mechanical output work. Two components of the system have been developed: (1) the external combustion micro heat engine and (2), a thermal switch to control heat transfer to and from the heat engine.

As shown in Figure 1, the engine consists of a cavity filled with saturated working fluid. The cavity is defined by two membranes. The bottom membrane serves as an evaporator. The top membrane serves as an expander. An SU8 wicking structure is fabricated on the bottom membrane to control the amount of working fluid available for evaporation. The wicking structure maintains a thin layer of working fluid across the bottom membrane by pumping liquid through the radial channels via capillary force.

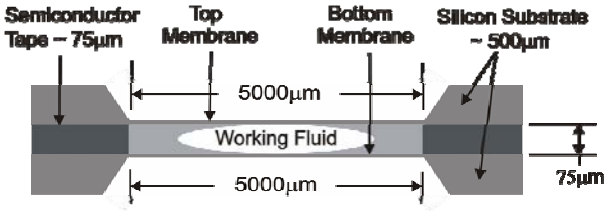

Figure 1: Engine Cross-Section

The engine is designed to operate by the intermittent addition and rejection of heat to/from the working fluid within the engine cavity. The theoretical Carnot efficiency for this device is about 5% due to the limited temperature excursions of the engine's working fluid and the ability to heat and cool it over a 10°C temperature gradient. Heat addition is accomplished via resistance heater fabricated on the bottom evaporator membrane. Heat rejection is accomplished via a thermal switch which periodically conducts heat through the bottom evaporator membrane. Making and breaking contact then effectively turns heat conduction from the engine on and off. When electrical power is dissipated in the resistance heater on the evaporator membrane, working fluid in the wicks is evaporated. This causes a pressure increase within the cavity of the engine and leads to expansion of the upper membrane and mechanical work. The thermal switch, which is always in contact with a cold source, then temporarily contacts the bottom membrane so heat may be transferred out of the engine and vapor-phase working fluid may condense on the evaporator membrane in the engine cavity.

Previous work leading to the development of a thermal switch based on an array of liquid-metal micro-droplets is described in [4]. This work also demonstrated a thermal switch with a thermal resistance of 1°C/W for the "on" state and 100°C/W for the "off" state. Integration of such a thermal switch with the micro heat engine presented here has previously shown the engine to operate at speeds up to 100Hz [5].

Previous work in our lab has also shown that increased upper membrane compliance results in increased mechanical output

Copyright © 2006 by ASME

Downloaded From: https://proceedings.asmedigitalcollection.asme.org on 06/29/2019 Terms of Use: http://www.asme.org/about-asme/terms-of-use

from and efficiency of the engine [6]. The present work extends this study by considering the effect of three different 5mm square top membranes on engine output; a 2micron thick silicon membrane, a 300nm thick silicon-nitride membrane, and a 3micron thick corrugated silicon membrane. In particular, the present work focuses on the effect of top membrane compliance on engine mechanical power and efficiency.

EXPERIMENT

Figure 2 shows the experimental apparatus used in these experiments. The experimental setup included the engine, which consisted of top and bottom 5mm square membranes, and the thermal switch, which intermittently contacted the bottom engine evaporator membrane. The engine evaporator membranes were fabricated via anisotropic wet etch using silicon etched to a thickness of 2microns. A thin-film layer of gold was patterned to form a resistance heater on the membrane surface. Capillary wicks were fabricated atop the heater using SU8 patterned via photolithography to define the wicking channels.

Three types of top membranes were fabricated: silicon, silicon-nitride, and corrugated silicon. The silicon membranes were fabricated by wet-etching silicon wafers to a thickness of 2microns. The silicon-nitride membranes were fabricated by depositing a 300nm layer of silicon-nitride on top of a silicon wafer. The silicon was then wet etched to leave only the silicon-nitride membrane. The corrugated silicon membranes were fabricated in a multi-step protocol. First, trenches (which later formed the corrugated part of the membrane) were formed by a timed etch in an ethylene diamine pyrocatechol (EDP) solution through an oxide mask to a depth of approximately 15microns. After the etch, the oxide mask was stripped and a 3micron p^{++} etch stop was formed over the entire wafer by boron diffusion from a solid source. All oxides were then removed and 150nm of oxide was regrown in a wet oxygen environment. Square windows were then etched in the oxide on the side opposite the shallow trenches and bulk silicon removal was performed in EDP until stopping on the p^{++} layer. This etch resulted in 3micron thick corrugated silicon membranes. This fabrication procedure produced four corrugated trenches located at an outer radius of 4.8mm on the square 5mm membrane.

The thermal switch contacting the bottom membrane of the engine consisted of a liquid-metal droplet array deposited via physical vapor deposition on a silicon die. The micro-droplet arrays were fabricated with 30micron droplets formed by the preferential condensation of mercury vapor on circular gold targets. The targets were arranged in a 40 by 40 array, resulting in 1600 micro-droplets after deposition. The droplet array die was then mounted on a constant temperature heat sink resting above a piezo-stack actuator. The piezo actuator used was able to translate the droplet array 80microns at 200Hz.

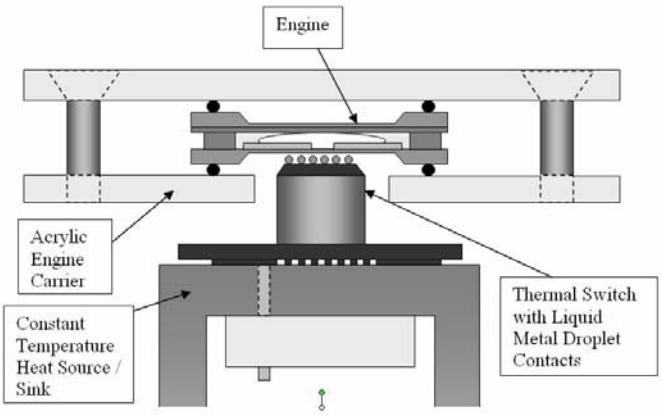

Figure 2: Engine and Thermal Switch

To assemble the engine, an expander membrane and bottom evaporator membrane were clamped face to face with a 75micron semi-conductor tape gasket between them. The resulting cavity was filled with 3M™ PF-5060DL refrigerant to serve as the working fluid. This assembly was then placed above the thermal switch.

Heat addition to the engine was accomplished by dissipating electrical power in the evaporator membrane's resistance heater. Heat rejection was controlled by the thermal switch which was cooled to a temperature of 15 °C and brought into contact with the evaporator membrane during heat rejection. Thus the operating temperature difference between the switch and engine was 25 °C. The temperature of the thermal switch was monitored by a fine-wire thermocouple

Three different top expander membranes were tested during these experiments with engines operating at 20, 40, and 100Hz. In the first configuration, the engine was operated using a 2micron thick silicon top membrane. In the second configuration, the engine was operated using a 300nm thick silicon-nitride membrane. In the third configuration, the engine was operated using a 3micron thick silicon corrugated upper membrane.

The mechanical work of the engine was taken to be the boundary work performed by the top expander membrane. A laser vibrometer was used to monitor the deflection of the top membrane. Engine efficiency was defined to be the mechanical work out of the engine divided by the electrical work dissipated in the resistance heater on the evaporator membrane. The work required to actuate the thermal switch was not accounted for in these efficiency calculations. The actuator used for the thermal switch required 300mW to operate at 40Hz and 800mW to operate at 100Hz. In more recent experiments, a cantilever thermal switch was designed such that switch operation required only 100μW at 100Hz.

Because the thermal switch was mechanically actuated into contact with the evaporator membrane of the engine, care was

Copyright © 2006 by ASME

Downloaded From: https://proceedings.asmedigitalcollection.asme.org on 06/29/2019 Terms of Use: http://www.asme.org/about-asme/terms-of-use

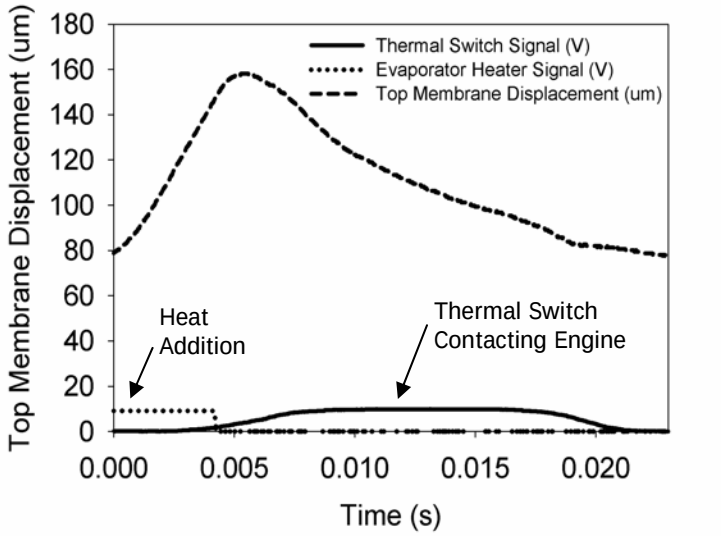

Figure 3. Typical Engine Operation at 40Hz

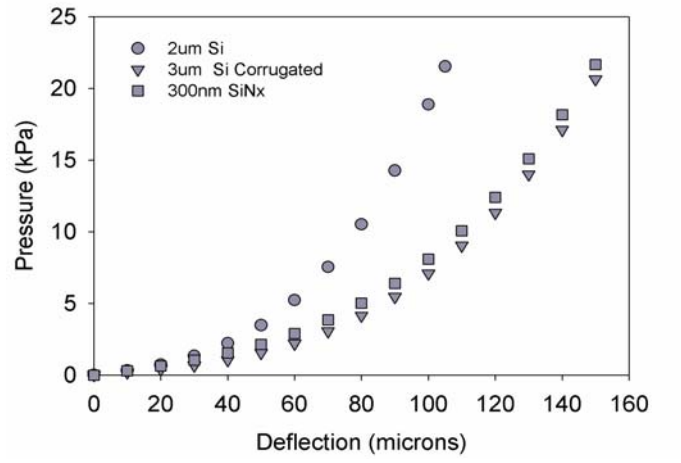

Figure 4: Pressure-Deflection Curves for 3 Membranes

taken to limit the force of contact between the two. In this manor, the work output of the upper membrane did not benefit from the mechanical action of the thermal switch.

RESULTS

Figure 3 shows the typical operating signals to and from an engine operating at 40Hz. The thermal switch is actuated to make contact with the engine after the top membrane has reached its maximum displacement at the end of the heat addition process.

Figure 4 shows the pressure-deflection curves of the three membranes tested as top membranes. Both the silicon-nitride and corrugated silicon membranes showed increased deflection at a given pressure as compared to the plain silicon membranes.

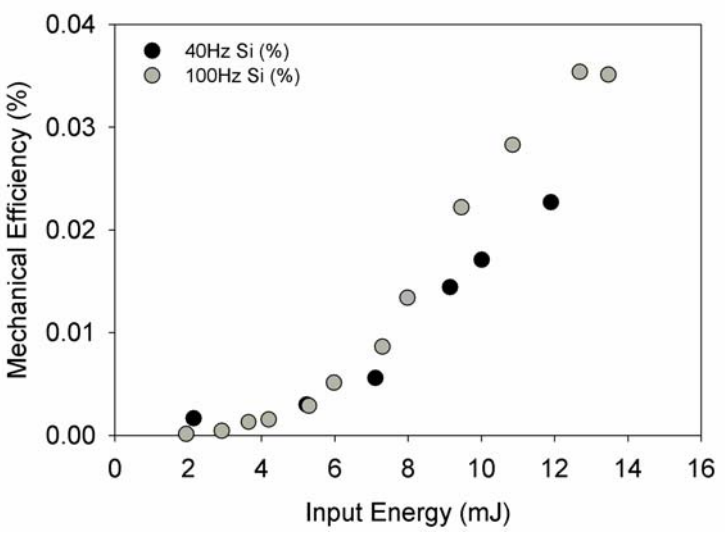

Figure 5: Silicon Upper Membrane Mechanical Efficiency

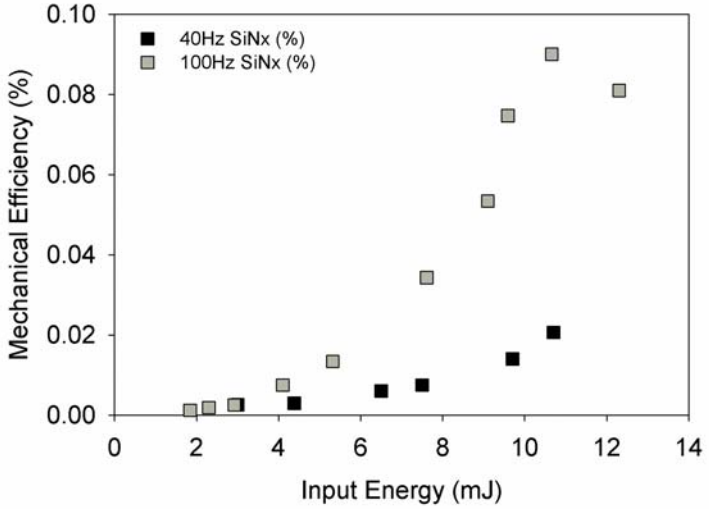

Figure 6: SiNx Upper Membrane Mechanical Efficiency

Figure 5 shows the mechanical efficiency of the engine operated with a 2um thick upper silicon membrane. Data is given for operation at 40 and 100Hz. The maximum efficiency achieved using a silicon membrane was .035% at 100Hz.

Figure 6 shows the mechanical efficiency of the engine operated with a 300nm thick silicon-nitride upper membrane. Data is given for operation at 40 and 100Hz. The maximum efficiency achieved using a silicon-nitride upper membrane was slightly below .10% at 100Hz. The use of the more compliant silicon-nitride membrane resulted in an increase in efficiency over the two-micron silicon membrane.

Copyright © 2006 by ASME

Downloaded From: https://proceedings.asmedigitalcollection.asme.org on 06/29/2019 Terms of Use: http://www.asme.org/about-asme/terms-of-use

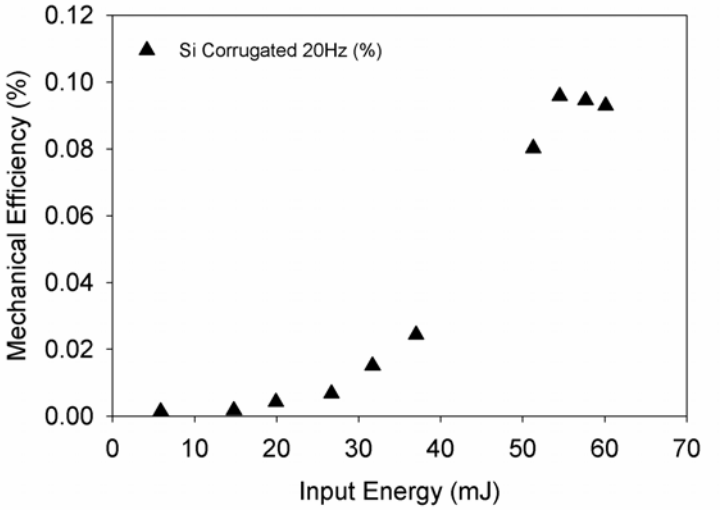

Figure 7: Si Corrugated Upper Membrane Mechanical Efficiency

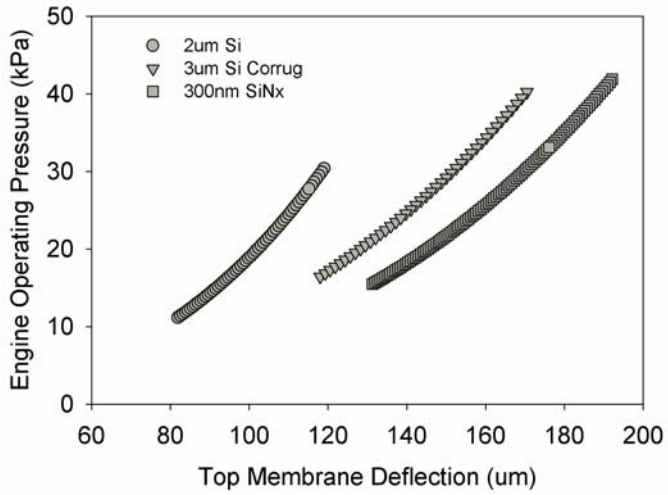

Figure 8: Operating Pressure and Top Membrane Displacement

Figure 7 shows mechanical efficiency of the engine operated with a 3micron thick corrugated silicon upper membrane. In this case data is given for operation at 20Hz. The maximum efficiency attained was .09% at 20Hz.

The trend of increased upper membrane compliance with increased engine operating efficiency was also evident in the operating pressure curves of these three engines. Figure 8 shows the cyclic change of both working pressure and top membrane deflection of the three engines operating at 100Hz. 10.5mJ of heat was applied per cycle for all engines. The silicon-nitride and corrugated silicon top membranes showed increased deflection and increased pressure differential as compared to the plain silicon top membrane. The greatest pressure differential achieved for all tests was measured to be 42kPa for the case of the silicon-nitride upper membrane.

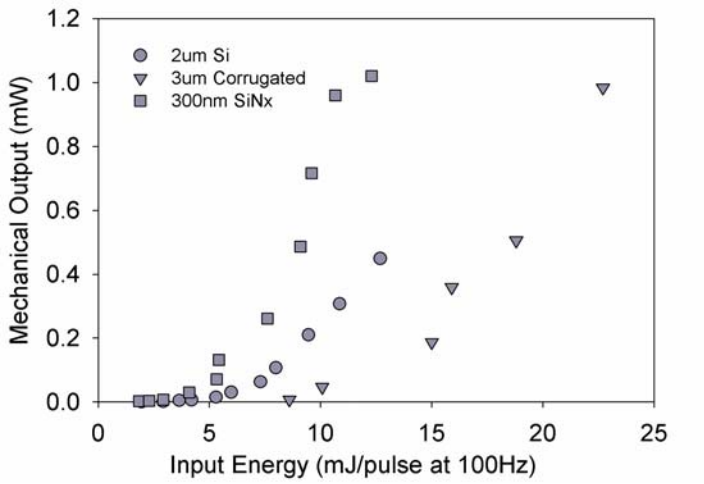

Figure 9: Mechanical Power Output at 100Hz

Maximum change in top membrane deflection was found to be 43microns, also for the engine constructed with a silicon-nitride upper membrane.

Figure 9 shows a plot of mechanical power output from the engine versus energy dissipated in the resistance heater during one heat addition cycle. The figure shows that increased top membrane compliance via thin silicon-nitride or corrugated silicon membranes increases mechanical power output from the engine from .45mW to 1.0mW. The maximum mechanical power output was 1.0mW for both the case of the 300nm thick silicon-nitride upper membrane and the 3um thick corrugated membrane.

SUMMARY AND CONCLUSIONS

The effect of top membrane compliance on the operation of an external combustion micro-heat engine with integrated thermal switch has been documented. The increased compliance of top engine membranes produced improved operating efficiency and power output from the engine. The use of a 2micron thick silicon upper membrane on the engine produced .45mW of mechanical power and achieved a maximum mechanical efficiency of .035%. Mechanical power output was measured to be 1.0mW from a 300nm thick silicon-nitride top membrane operating at a mechanical efficiency of .10%. Mechanical power output was measured to be 1.0mW for an engine operated with a 3micron thick corrugated upper membrane with a maximum mechanical efficiency of .09%.

REFERENCES

[1] A. Mehra, X. Zhang, A.A. Ayon, I.A., Waitz, M.A., Schmidt and C.M. Spadaccini, “A Six-Wafer Combustion System for a Silicon Micro Gas Turbine Engine,” J.MEMS, Vol.9, No. 4 (2000)

Copyright © 2006 by ASME

Downloaded From: https://proceedings.asmedigitalcollection.asme.org on 06/29/2019 Terms of Use: http://www.asme.org/about-asme/terms-of-use

[2] H. T. Aichlmayr, D. B. Kittelson, and M. R. Zachariah. "Miniature free-piston homogeneous charge compression ignition engine-compressor concept—Part I: performance estimation and design considerations unique to small dimensions," Chemical Engineering Science Vol.57 (2002)

[3] K. Fu, A. J. Knobloch, F.C. Marinez, D.C. Walther, C. Fernandez-Pello, A.P. Pisano, D. Liepmann, "Design and Fabrication of a Silicon-Based MEMS Rotary Engine," *Proc. ASME IMECE 2001*, Paper No. MEMS-23925, New York (2001).

[4] T. S. Wiser. "Steady State Heat Transfer Characterization of a Liquid-Metal Thermal Switch," MS Thesis, Washington State University, 2005.

[5] L. W. Weiss, J.H. Cho, K. E. McNeil, D.F. Bahr, C.D. Richards and R.F. Richards. "Characterization of a dynamic micro heat engine with integrated thermal switch." Journal of Micromechanics and Microengineering. 2006, 16 S262-S269

[6] S.A. Whalen, D.F. Bahr, C.D. Richards, and R.F.Richards, "Characterization of a Liquid-Vapor Phase-Change Actuator," Proc. of ASME IMECE, Florida, U.S.A., Nov. 5-11, 2005, Paper No. IMECE-82564

Copyright © 2006 by ASME

Downloaded From: https://proceedings.asmedigitalcollection.asme.org on 06/29/2019 Terms of Use: http://www.asme.org/about-asme/terms-of-use